

Supporting Information

A microporous Cu-MOF with optimized open metal sites and pore spaces for high gas storage and active chemical fixation of CO₂

Contents

S1. Materials and Methods

S2. Supplementary tables and figures

S3. The NMR spectrums

S4. References

S1. Materials and Methods

All the chemicals were obtained from commercial sources, and were used as received except H₄L. The organic ligand H₄L was synthesized by 3, 5-dimethyl-bromobenzene and dimethyldichlorosilane. Deionized water was used for all experiments. Elemental analyses (C, H and N) were measured on a Perkin-Elmer 2400 CHN elemental analyzer, Thermogravimetric analysis (TGA) was made using a SDT 2960 Simultaneous DSC-TGA of TA instruments up to 800 °C, and the heating rate was 10 °C min⁻¹ under an air flow. Powder X-ray power diffraction (XRD) patterns were performed on a D8 Focus (Bruker) diffractometer with Cu K radiation Field-emission ($\lambda = 0.15405$ nm, continuous, 40 kV, 40 mA, increment = 0.02°).

S1.1 Synthesis of bis(3,5-dimethylphenyl)dimethylsilane

n-BuLi (2.5M in hexanes, 43.23 mL, 108.07 mmol) was added to a solution of 3,5-dimethyl-bromobenzene (20.00 g, 108.07 mmol) in 120 mL Et₂O at 0 °C and stirred for 3 hours. Then dimethyldichlorosilane (6.83 g, 52.96 mmol, 6.39 mL) was dissolved with 20 mL Et₂O and added dropwise at 0 °C. The reaction mixture was slowly warmed to room temperature and stirred overnight. After being quenched with 100 mL of H₂O, the organic layer was separated, washed with brine, and dried over anhydrous Mg₂SO₄. Removal of the solvents under vacuum to give yellow oil, which was purified by silica gel column to give pure product (13.50 g, 94.9%). ¹HNMR (CDCl₃, 400MHz) δ /ppm: 7.13 (s, 4H, ArH), 7.00 (s, 2H, ArH), 2.30 (s, 12H, Ar-CH₃), 0.50 (s, 6H, Si-CH₃).

S1.2 Synthesis of 5,5'-(dimethylsilanediyl) diisophthalic acid

A 1L three-neck round flask was charged with bis(3,5-dimethylphenyl)dimethylsilane (8 g, 22.31 mmol), 70 ml of water and 200 ml pyridine. The mixture was heated to reflux and KMnO₄ (126.92 g, 0.80mol) was partly added, and then the reaction mixture was stirred for 24h. The reaction mixture was cooled to room temperature and 150 mL of CH₃OH was added slowly to decompose unreacted KMnO₄. Manganese dioxide was removed by vacuum filtration and the solid was washed with hot water. The filtrate was concentrated on a hot-plate to about 30 ml and concentrated HCl was added until the pH was 1. The resulting white solid was dissolved in dilute aqueous NaOH. The solution was filtered and reacidified with concentrated HCl. The new solid was collected and dried: 6.70 g (55.8%). ¹HNMR (CDCl₃, 400MHz) δ /ppm: 13.33 (s, 2H), 8.49 (t, J = 1.6 Hz, 1H), 8.26 (d, J = 1.6 Hz, 2H), 0.67 (s, 3H).

S1.3 Synthesis of compound 1

A solution of CuCl₂•4H₂O (21 mg, 0.10 mmol) and H₄L (17 mg, 0.05 mmol) in a mixture of DMF (3 mL) and H₂O (3 mL) in a capped 20 mL glass vial was heated at 70 °C for 3 days, affording green hexagon crystals in a ca. 70% yield based on H₄L.

Elemental analysis for C₂₄H₃₄O₁₄N₂Cu₂Si: C, 40.27%; H, 4.78%; N, 1.96%. Found: C, 40.23%; H, 4.81%; N, 1.93%. Selected IR data (cm⁻¹, Fig. S, ESI): 2935 (w), 1655 (s), 1621 (s), 1409 (s), 1354 (s), 1251 (m), 1197 (w), 1087 (m), 881 (m), 814 (m), 766 (m), 725 (m), 649 (w).

The agreement between the experimental and simulated PXRD patterns indicated the phase purity of the as-synthesized product.

S1.4 Single Crystal X-ray Structure Determination

Suitable single crystal of **1** was selected for single-crystal X-ray diffraction analysis. Crystallographic data collections were performed on collected a Bruker Apex II CCD diffractometer with graphite monochromated Mo-K α radiation ($\lambda = 0.71073 \text{ \AA}$) at 293 K. Data processing was accomplished with the SAINT processing program.¹ The structure was solved by the direct methods and refined by full-matrix least-squares fitting on F^2 using the SHELXTL crystallographic software package.² Non-hydrogen atoms were refined with anisotropic displacement parameters during the final cycles. All hydrogen atoms of the organic molecule were placed by geometrical considerations and were added to the structure factor calculation. The guest molecules were disordered and could not be modelled properly, the diffused electron densities resulting from them were removed by the SQUEEZE routine in PLATONS3 and the results were appended in the CIF file. The reported refinements are of the guest-free structures using the *.hkp files produced using the SQUEEZE routine. The final formula of **1** was determined by single-crystal X-ray diffraction, thermogravimetric and elemental analyses. Crystallographic data for **1** (1483155) has been deposited with Cambridge Crystallographic Data Centre. Data can be obtained free of charge upon request at www.ccdc.cam.ac.uk/data_request/cif. Crystal data and structure refinement is summarized in Table S1. Topology information for **1** was calculated by TOPOS 4.0.³

S1.5 Gas adsorption measurements

The N₂, H₂, CH₄ and CO₂ adsorption measurements were performed on automatic volumetric adsorption equipment (Quantachrome Autosorb-iQ). Prior to gas adsorption measurements, the as-synthesized samples were immersed in methanol for 3 days; during the exchange the methanol was refreshed three times remove the non-volatile DMF solvates. The resulting methanol-exchanged sample of **1** was transferred as a suspension to a Buchner funnel and the solvent was decanted. Then the samples were degassed under a dynamic vacuum at 100 °C for 10 hours. A colour changed from bright-blue to deep purple-blue is a typical feature for Cu paddlewheel to generate open Cu sites.

S1.6 Fitting of pure component isotherms

Experimental data on pure component isotherms for CO₂, CH₄, N₂ and H₂ were fitted by dual-site Langmuir-Freundlich (DSLFF) adsorption model⁴. The DSLFF model is described as:

$$N = \frac{N_1 b_1 P^{1/n_1}}{1 + b_1 P^{1/n_1}} + \frac{N_2 b_2 P^{1/n_2}}{1 + b_2 P^{1/n_2}} \quad (1)$$

In equation (1), P is the pressure of bulk gas at equilibrium with adsorbed phase; N_1 and N_2 are the maximum loading in sites 1 and 2; b_1 and b_2 are the affinity constants of sites 1 and 2; n_1 and n_2 are used to characterize the deviation from the single Langmuir equation. The fits are excellent for all components over the entire pressure range.

S1.7 IAST calculations of adsorption selectivities

The selectivity of preferential adsorption of component 1 over component 2 in a mixture containing 1 and 2 can be formally defined as:

$$S_{ads} = \frac{q_1/q_2}{p_1/p_2} \quad (2)$$

In equation (2), q_1 and q_2 are the absolute component loadings of the adsorbed phase in the mixture. These component loadings are also termed the uptake capacities. We calculate the values of q_1 and q_2 using the Ideal Adsorbed Solution Theory (IAST) of Myers and Prausnitz.⁵

S1.8 The isosteric heats of adsorption

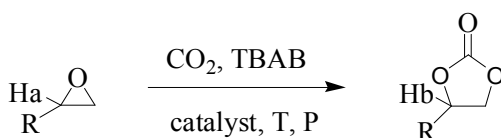
The isosteric heat of adsorption, Q_{st} , defined as:

$$Q_{st} = RT^2 \left(\frac{\partial \ln P}{\partial T} \right)_q \quad (3)$$

The equation (3) was determined using the pure component isotherm fits using the Clausius-Clapeyron equation, where P is pressure, T is temperature, q is the amount adsorbed, R is the gas constant, and Q_{st} denotes the heat of adsorption.

S1.9 Cycloaddition of CO₂ to Styrene Oxide

The conversion was calculated from ¹H NMR according to the following equation.



$$\text{conversion} = \frac{1\text{Hb}}{(1\text{Ha} + 1\text{Hb})}$$

S2. Tables and figures

Table S1. Crystal data and structure refinement for **1**.

Name	1
Empirical formula	C ₂₄ H ₃₄ O ₁₄ N ₂ Cu ₂ Si
Formula weight	729.7
Temperature (K)	173(2)
Wave length (Å)	0.71073
Crystal system	Hexagonal
Space group	<i>P6₃/mmc</i>
a (Å)	18.5185(5)
b (Å)	18.5185(5)
c (Å)	19.1215(11)
α(deg)	90
β(deg)	90
γ(deg)	120
Volume (Å ³)	5678.9(4)
Z, D _{calc} (Mg/m ³)	6, 0.953
Absorption coefficient (mm ⁻¹)	1.184
F (000)	1632
Crystal size (mm ³)	0.180 x 0.140 x 0.120
θ range (deg)	1.66 to 26.06
index range (deg)	-22<=h<=20, -22<=k<=22, -23<=l<=17
Reflections collected / unique	34876 / 2125 [R(int) = 0.0735]
Data / restraints / parameters	2125 / 0 / 80
Goodness-of-fit on F ²	0.996
R ₁ , wR ₂ (I > 2σ(I))	0.0419, 0.1199
R ₁ , wR ₂ (all data)	0.0561, 0.1278
Largest diff. peak and hole (e Å ⁻³)	0.385, -0.289

$$R_1 = \frac{\sum ||F_o| - |F_c||}{\sum |F_o|} \quad wR_2 = \left[\frac{\sum [w(F_o^2 - F_c^2)^2]}{\sum [w(F_o^2)]} \right]^{1/2}$$

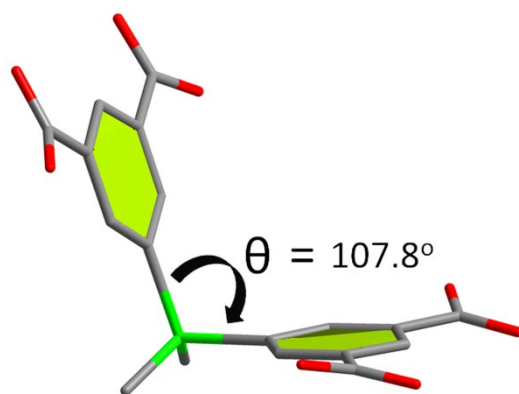


Figure S1 5,5'-(dimethylsilanediyl) diisophthalic acid ligand with dihedral angle in **1**.

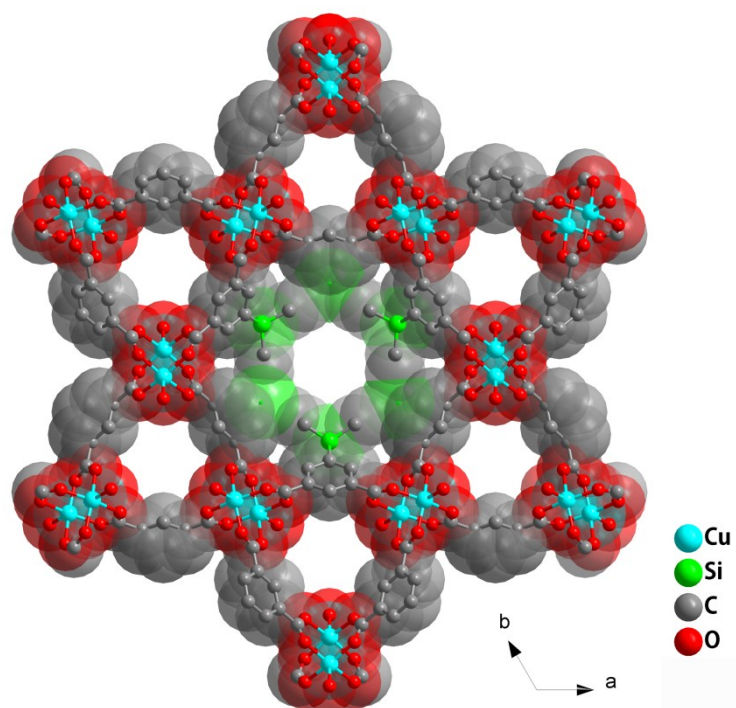


Figure S2 Space-filling view of the structure of **1** showing pores along the *c*-axis. For clarity the hydrogen atoms have been omitted.

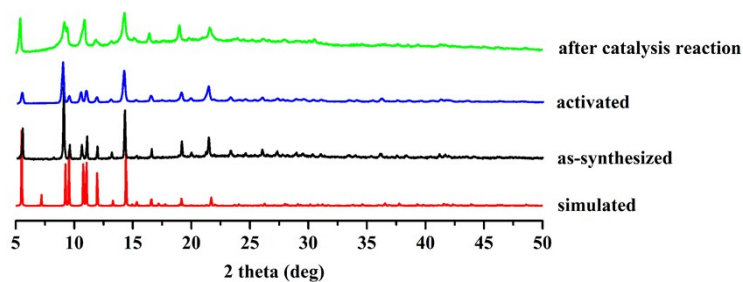


Figure S3 The simulated, as-synthesized and activated powder X-ray (PXRD) patterns for **1**.

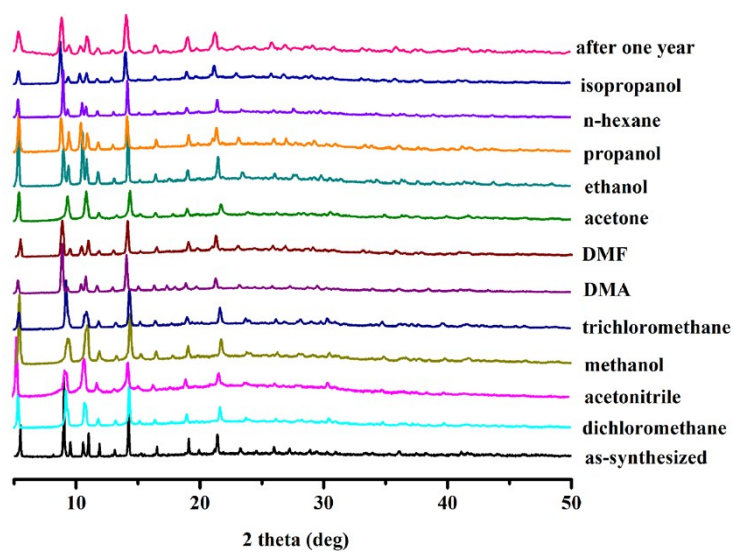


Figure S4 Powder X-ray diffraction patterns of as-synthesized **1**, samples obtained after immersing in various solvents for 24h and the ones exposed to air for one year.



Figure S5 A colour change from green to blue in case of activation.

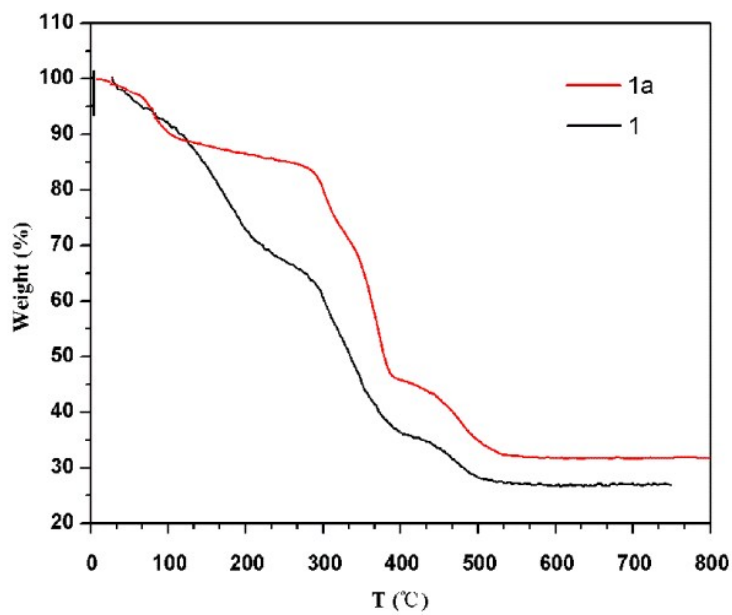


Figure S6 Thermogravimetric analysis (TGA) curves for the as-synthesized and activated samples of **1**. The curve of fresh samples show a weight loss of 37.12 % between room temperature and 300 °C, corresponding to the loss of coordinated H₂O molecules, guest H₂O and DMF molecules.

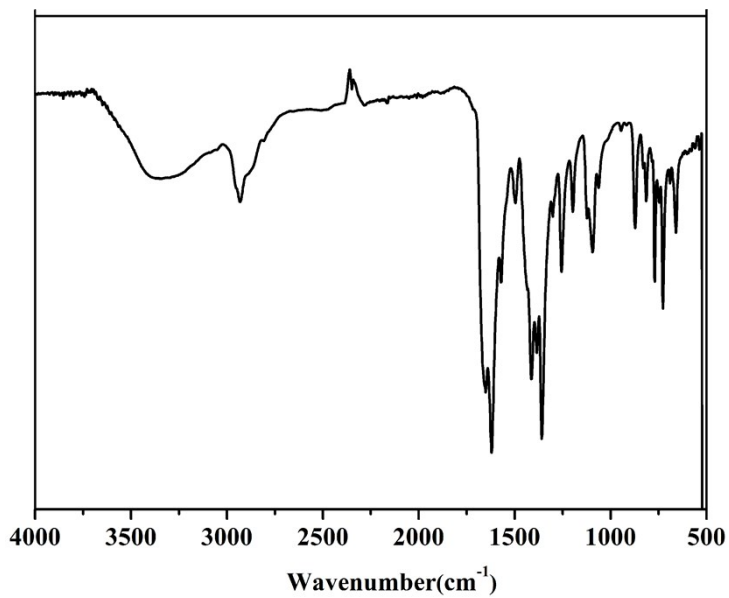


Figure S7 The infrared spectrum of **1**.

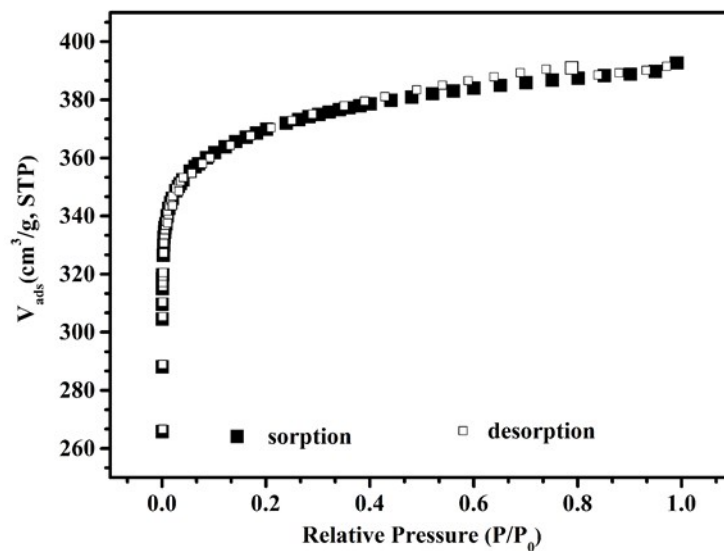


Figure S8 The N₂ sorption isotherm at 77K (P₀ = 101 KPa).

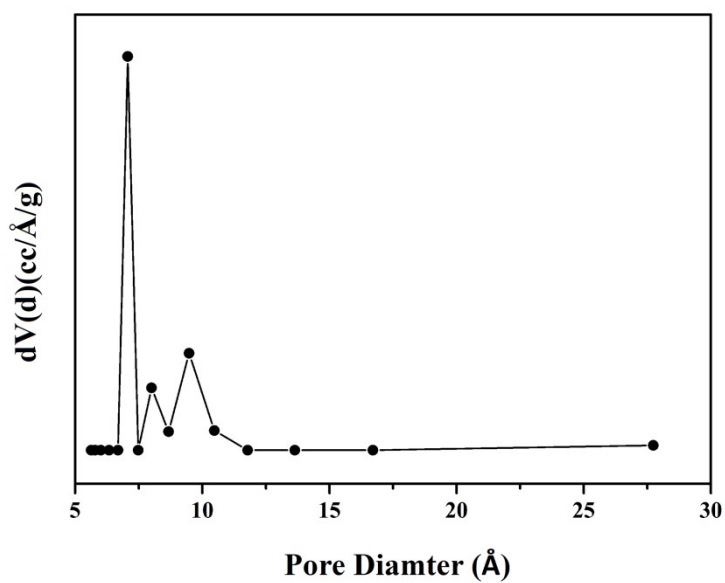


Figure S9 The pore size distribution calculated using the BJH method.

Temperature	Gas	Adsorption amount (at saturation)			
		cm ³ g ⁻¹	cm ³ cm ⁻³	mmol g ⁻¹	wt%
77 K	N ₂	392.7	404.1	17.5	49.1
	H ₂	303.6	312.4	13.6	2.7
87K	H ₂	209.5	215.5	9.4	1.9
273K	CO ₂	149	153.3	6.7	29.3
	CH ₄	69	71.0	3.1	4.9
298K	CO ₂	115.4	118.8	5.2	22.7
	CH ₄	18	18.5	0.8	1.3

Table S2 Gas adsorption data of 1a.

To predict the CO₂ separation behaviour of **1a** at 298K, ideal adsorbed solution theory (IAST)⁵ theory were employed for binary gas adsorption selectivity. The calculated CO₂/CH₄ and CO₂/N₂ selectivities are 8-11 and 25-35 from 1-100 KPa, respectively. The selectivity of **1a** for CO₂ over CH₄ and N₂ under these conditions is comparable to the majority of MOFs reported to date.⁶

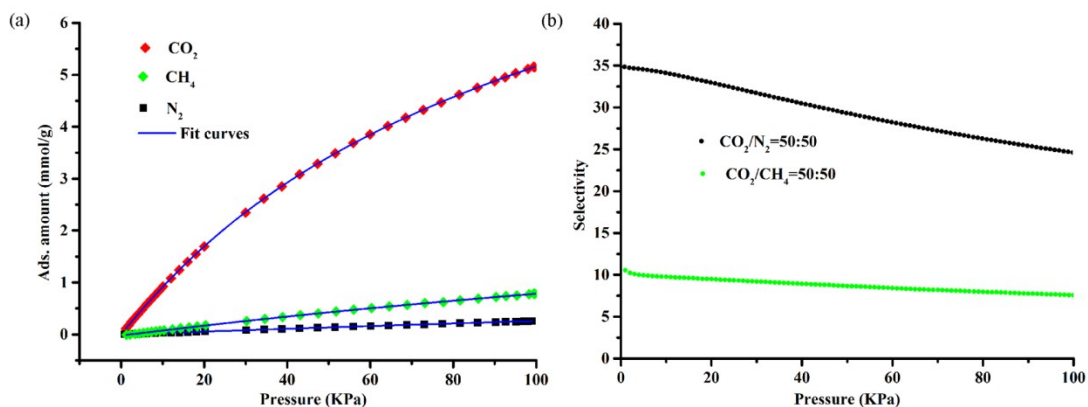


Figure S10. (a) CO₂, CH₄ and N₂ adsorption isotherms at 298 K along with the Dual-site Langmuir Freundlich (DSLFF) fits. (b) Gas mixture adsorption selectivities from equimolar CO₂/CH₄ and CO₂/N₂ mixtures predicted by IAST at 298K from 1- 100 kPa for **1a**.

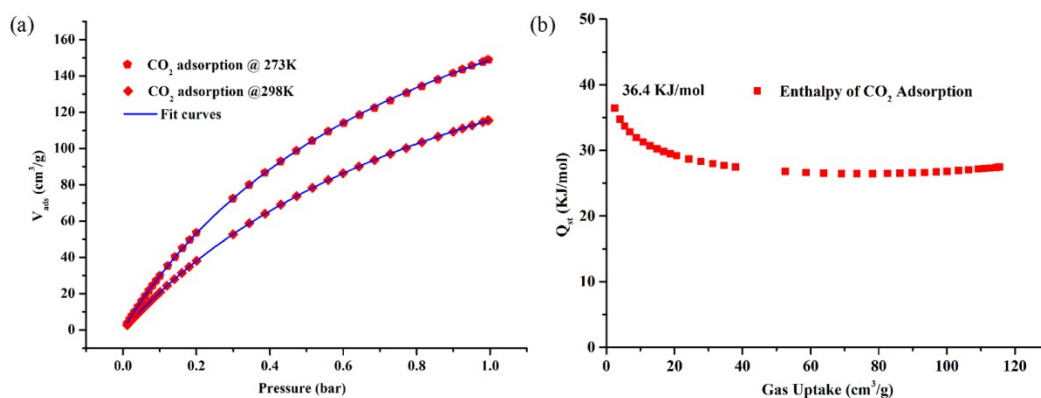


Figure S11. (a) CO₂ adsorption isotherms for **1a** fitted by the Langmuir-Freundlich equation. (b) Isotheric heat of CO₂ for **1a** calculated from the CO₂ adsorption isotherms at 273 and 298 K, employing the Clausius-Clapeyron equation.

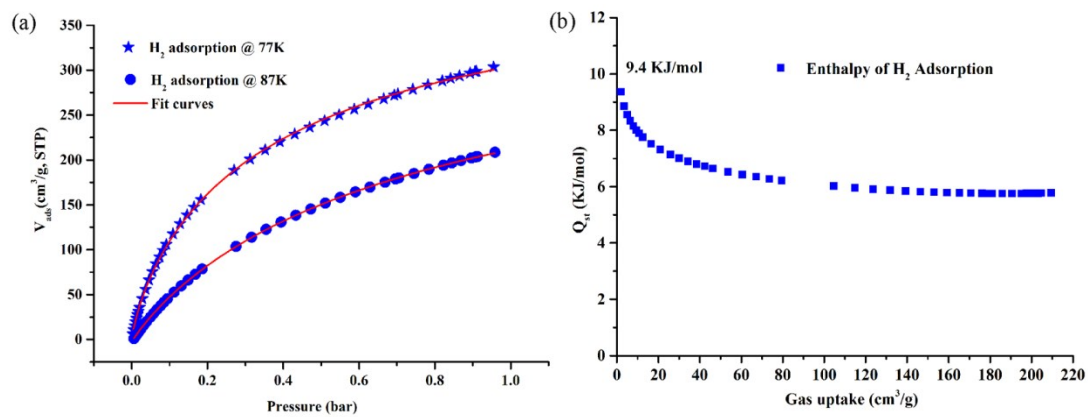


Figure S12. (a) H₂ adsorption isotherms for **1a** fitted by the Langmuir-Freundlich equation. (b) Isosteric heat of H₂ for **1a** calculated from the H₂ adsorption isotherms at 77 and 87 K, employing the Clausius-Clapeyron equation.

Compounds	SA _{BET} (m ² g ⁻¹)	H ₂ uptake (wt%)	References
[Cu(Me-4py-trz-	1473	3.07	7
PCN-12	1943	3.05	8
UTSA-20	1156	2.92	9
1a	1145.9	2.7	This work
NOTT-103	2929	2.63	10
In-soc-MOF	N.A.	2.60	11
NOTT-100	1670	2.59	10
L _{Cu'}	1952	2.57	11
PCN-11	1931	2.55	13
NOTT-101	2247	2.52	10
NOTT-105	2387	2.52	14
Cu(peip)	1560	2.51	15
JLu-Liu21	2080	2.5	16
PMOF-3	1879	2.47	17
NOTT-115	3394	2.42	18
NOTT-113	2970	2.39	18
PCN-10	1407	2.34	13
JLU-Liu20	1807	2.3	16
PMOF-2(Cu)	3730	2.29	19
Cu-BTT	1710	2.25	20
Mn-BTT	2100	2.42	20
MOF-74(Mg)	1510	2.2	21
UMCM-150	2300	2.1	22

N.A.: Not Available. The article does not list the data.

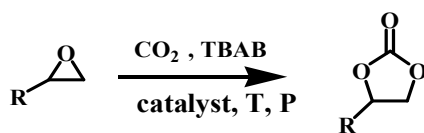
Table S3 The reported porous MOFs which exhibit over 2.0 wt% H₂ uptake at 77 K and 1 bar.

MOFs	CH ₄ uptake (cm ³ g ⁻¹)	Temperature(K)	References
1a	18	298	This work
	69	273	
JLU-Liu-20	31	273	20
	18	298	
JLU-Liu-21	37	273	16
	22	298	
L_{cu'}	36.97	273	12
	23.52	1.68	
CPM-33b	41.3	273	23
	26.5	298	

Table S4 Methane adsorption of **1a** and some reported MOFs at 1 bar.

Compounds	CO ₂ uptake (wt%)	Temperature (K)	References
SNU-5	38.5	273	24
1a	29.3	273	This work
Dy(BTC)	27.2	273	27
Cu₂(EBTC)(H₂O)₂	25.9	273	29
SNU-4	20.6	273	24
Mg-MOF-74	27.5	298	25
CPO-27-Mg	27.2	298	26
HKUST-1 (4 wt% H₂O)	27	298	28
Co-MOF-74	24.9	298	26
CPM-33b	24.8	298	23
Ni-MOF-74	23.9	298	25
1a	22.7	298	This work
PCN-6	18.9	298	29
HKUST-1 (8 wt% H₂O)	17.4	298	28
CPM-33c	17.4	298	23

Table S5 CO₂-uptake capacities of **1a** and some reported MOFs only with open metal sites at 1bar.



Entry	Substrate	Time (h)	conversion (%)	TON	TOF
1		2	>99	2000	1000
2		2	95.2	1904	952
3		2	65.8	1316	658
		4	86.2	1724	431
		6	>99	2000	333
4		2	31.3	626	313
		4	58.8	1176	294
		6	64.1	1282	214

Reaction conditions: epoxide (20 mmol), catalyst (0.01 mmol, based on $[\text{Cu}_2(\text{CO}_2)_4]$ cluster), and TBAB (0.3 mmol) under carbon dioxide (1 MPa) at 373 K. The yields were determined by ^1H NMR analysis.

Table S6 1a-catalyzed coupling of epoxides with CO_2 .

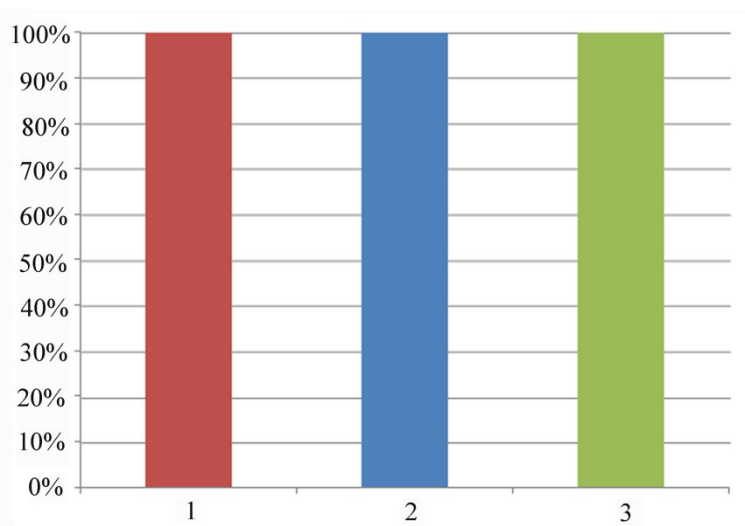


Figure S13 Histogram of recyclability study (three cycles) for catalytic activities of **1a** in coupling of glycidol with CO_2

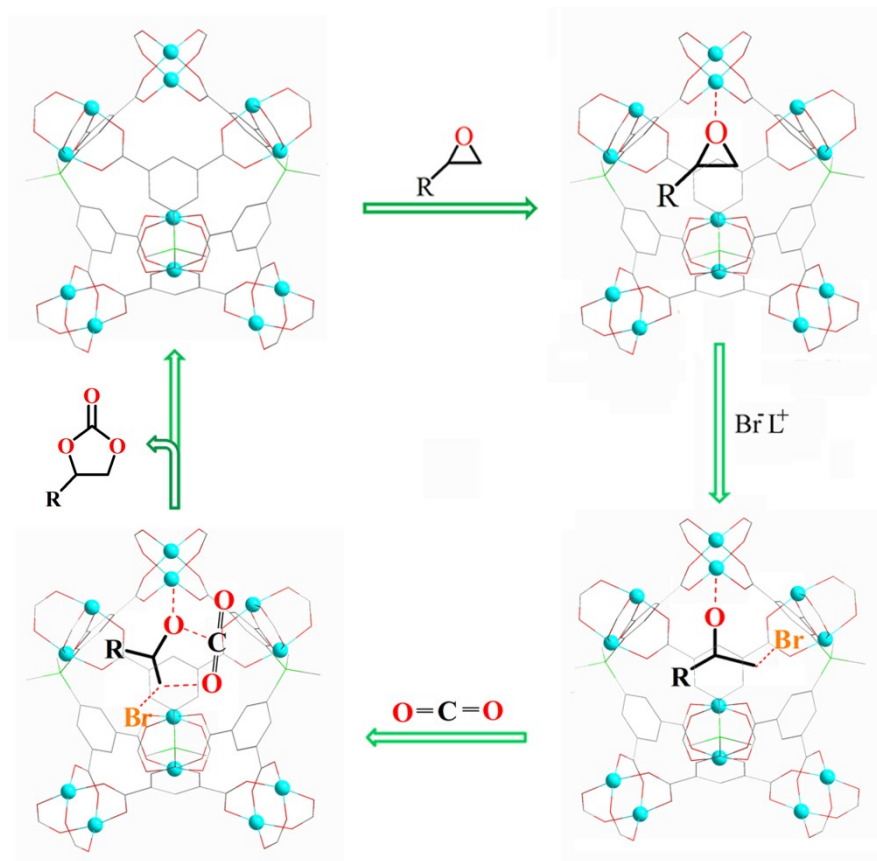


Figure S14 The proposed mechanism for the cycloaddition reaction of epoxide and CO₂ into cyclic carbonate catalyzed by **1a** (cyan sphere: open Cu site; L⁺ = tetra-*n*-butylammonium).

The MOF displays a high catalytic activity on CO₂ chemical fixation on account of its exposed Lewis-acid metal sites. As shown in the scheme, the coupling reaction is initiated by binding the epoxide with Lewis acidic copper sites. Once binding with copper, the C-O bond of epoxide is weakened due to part of electron transfer from the oxygen atom to copper. Subsequently, the less-hindered carbon atom of epoxide is attacked by the Br⁻ generated from *n*Bu₄NBr to open the epoxy ring as a consequence of its lower steric effect and higher positive charge. This is followed by the interaction of oxygen atom from CO₂ with the positively charged carbon and that of O atom of epoxide with the C atom of CO₂. The succedent ring closure gives the production of cyclic carbonate.

Entry	Cata.	T (°C)	P (MPa)	T (h)	TON	TOF	Ref.
1	1a	100	1.0	2	1904	952	This work
2	Gea-MOF-1	120	2.0	6	593	99	31
3	CHB (M)	120	1.2	6	44.6	7.4	34
4	Ni(salphen)-MOF	80	2.0	4	300	75	32
5	MOF-5	50	0.1	12	22.3	1.9	35
6	[Cu₄(L1)]_n	25	0.1	48	425	8.9	36

Table S7 Comparison with different MOF catalysts in the cycloaddition of CO₂ and epichlorohydrin.

Entry	Cata.	T (°C)	P (MPa)	T (h)	TON	TOF	Ref.
1	1a	100	1.0	6	2000	333	This work
2	Ni-TCPE1	100	1.0	12	2000	167	30
3	Ni(salphen)-MOF	80	2.0	4	196.4	49.1	32
4	CHB (M)	120	1.2	6	44	7.3	33
5	MOF-5	50	0.1	3	13.4	4.5	35

Table S8 Comparison with different MOF catalysts in the cycloaddition of CO₂ and 1,2-epoxy-3-phenoxypropane.

Entry	Cata.	T (°C)	P (MPa)	T (h)	TON	TOF	Ref.
1	1a	100	1.0	6	1282	214	This work
2	Ni-TCPE1	100	1.0	12	2000	166.7	30
3	Ni-TCPE2	100	1.0	12	1720	143.3	30
4	Gea-MOF-1	120	2.0	6	567	94.5	31
5	Ni(salphen)-MOF	80	2.0	4	289.3	72.3	32
6	<i>L_{Cu}'</i>	120	2.0	6	286	47.7	12
7	Co-MOF-74	100	2.0	4	28.8	7.2	33
8	CHB(M)	120	1.2	6	34.7	5.8	34

Table S9 Comparison with different MOF catalysts in the cycloaddition of CO₂ and styrene oxide under heating conditions.

S3. The NMR spectra

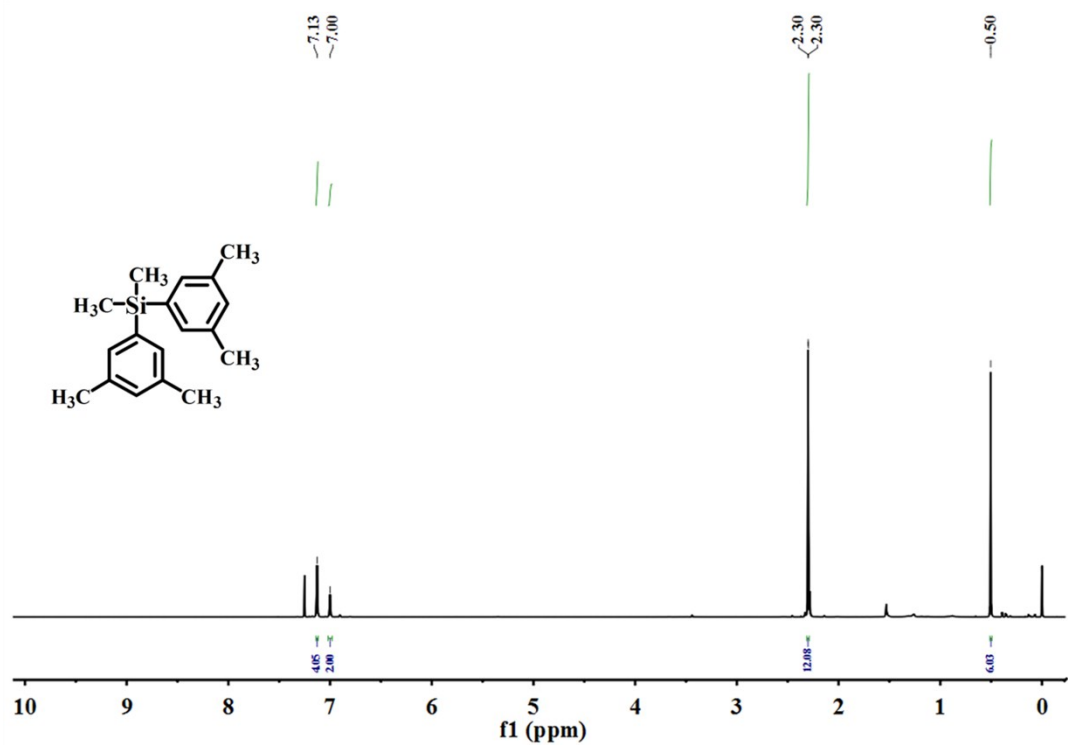


Figure S15 The ^1H NMR spectrum of (3,5-dimethyl-phenyl)-dimethyl-silane (400 MHz, CDCl_3): $\delta = 7.13$ (s, 4H, Ar-H), 7.00 (s, 2H, Ar-H), 2.31 – 2.29 (m, 12H, Ar- CH_3), 0.50 (s, 6H, Si- CH_3).

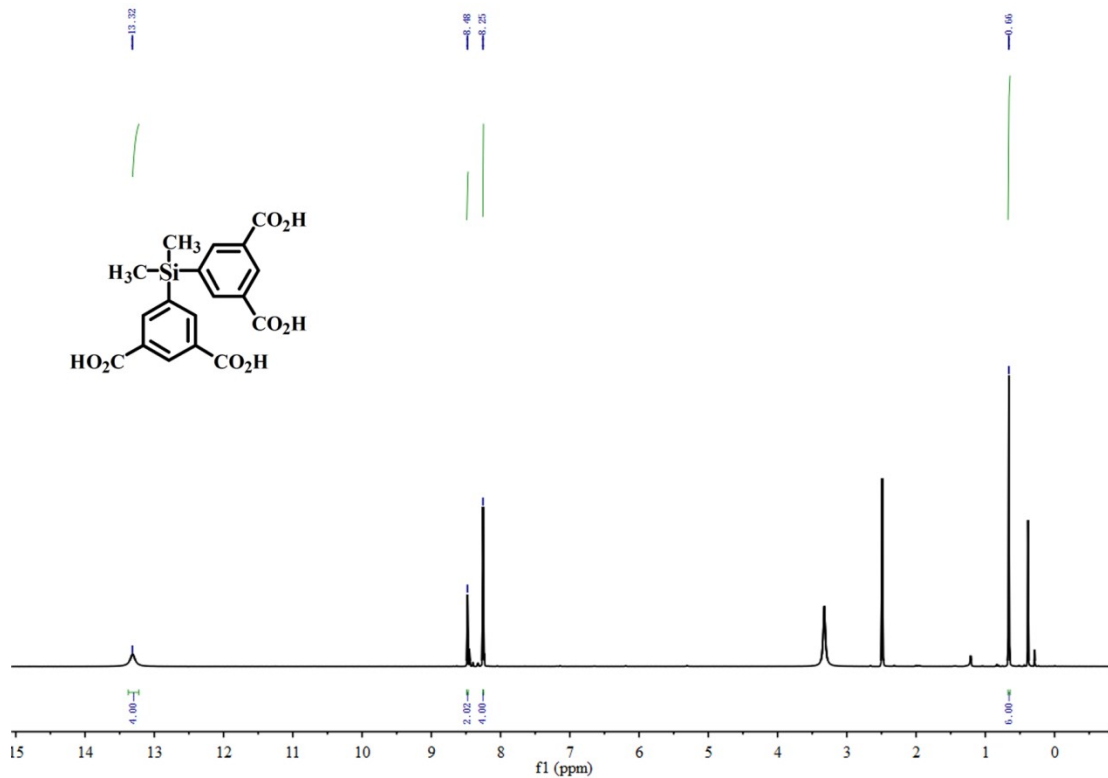


Figure S16 The ^1H NMR spectrum of H_4L (400 MHz, DMSO): $\delta = 13.33$ (br, 4H, -COOH), 8.49 (t, $J = 1.6$ Hz, 2H, Ar-H), 8.26 (d, $J = 1.6$ Hz, 4H, Ar-H), 0.67 (s, 6H, Si- CH_3).

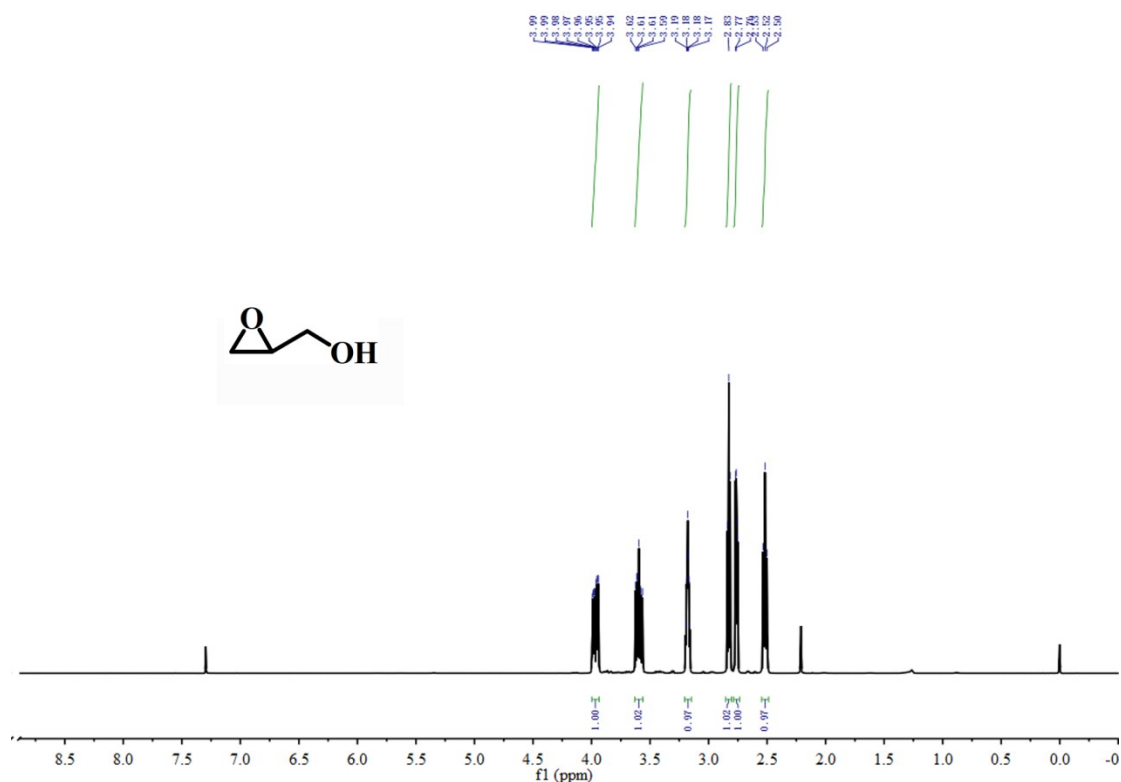


Figure S17 ^1H NMR spectra of glycidol (400 MHz, CDCl_3): δ = 3.94 – 3.99 (m, 1H, HO- CH_2), 3.56 – 3.62 (m, 1H, HO- CH_2), 3.16 – 3.19 (m, 1H, O-CH), 2.83 (t, J = 4.0 Hz, 1H, O- CH_2), 2.76 (q, J = 4.0 Hz, 1H, O- CH_2), 2.52 (t, J = 4.0 Hz, 1H, -OH).

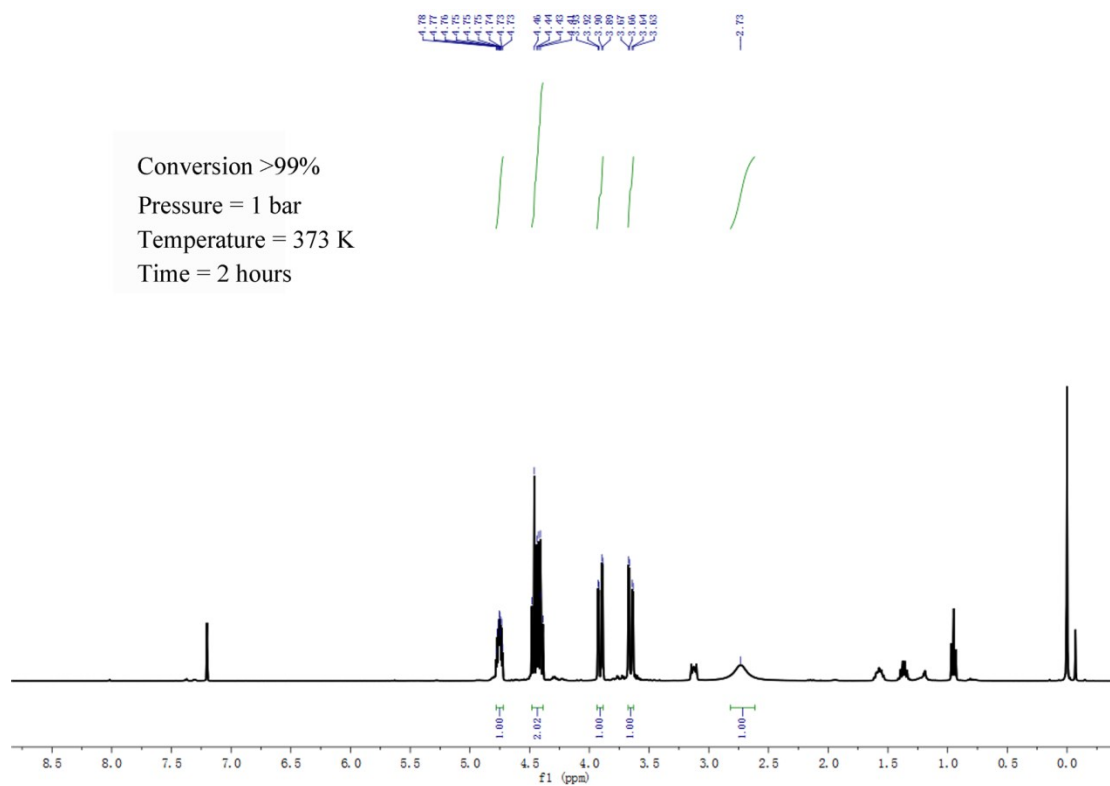


Figure S18 ^1H NMR spectra of the cycloaddition product of cyclopropyl-methanol with CO_2 (400 MHz, CDCl_3): δ = 4.73 – 4.78 (m, 1H, COO-CH), 4.39 – 4.48 (m, 2H, HO- CH_2), 3.91 (dd, J = 12.0 Hz, 4.0 Hz, 1H, COO- CH_2), 3.65 (dd, J = 12.0, 4.0 Hz, 1H, COO- CH_2), 2.73 (br, 1H, -OH).

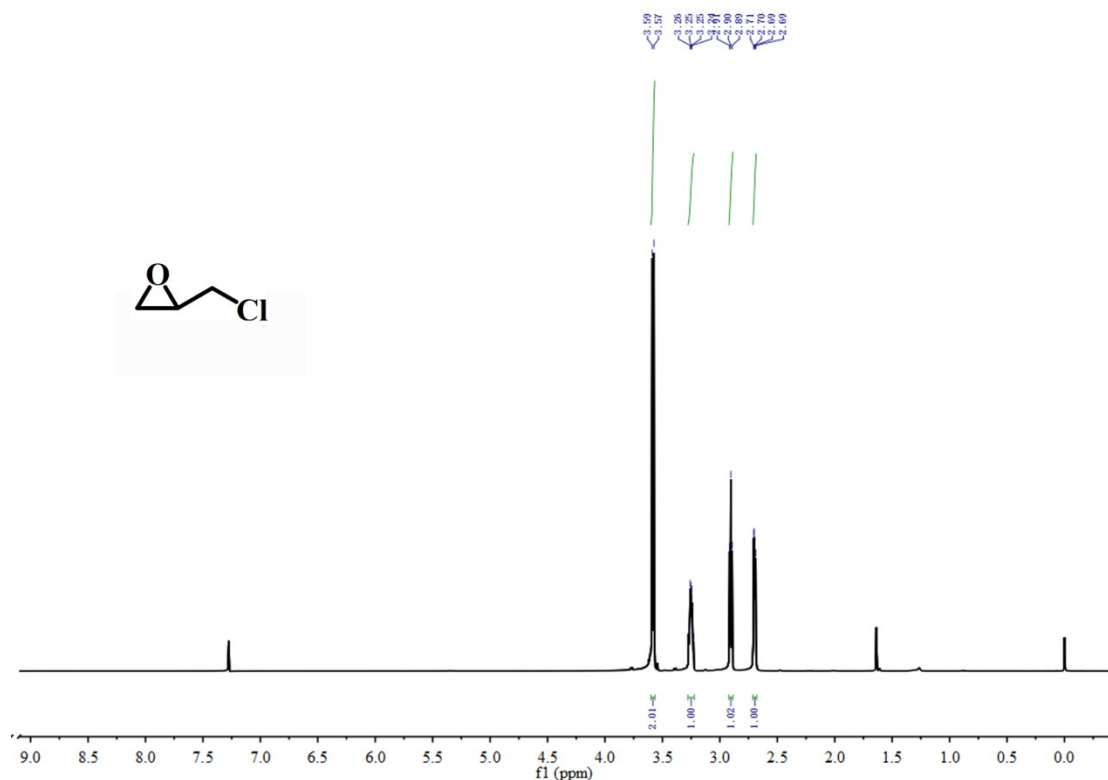


Figure S19 ^1H NMR spectra of chloromethyl-cyclopropane (400 MHz, CDCl_3): $\delta = 3.58$ (d, $J = 8.0$ Hz, 2H, Cl-CH_2), 3.23 – 3.27 (m, 1H, O-CH), 2.90 (t, $J = 4.0$ Hz, 1H, O- CH_2), 2.70 (q, $J = 4.0$ Hz, 1H, O- CH_2).

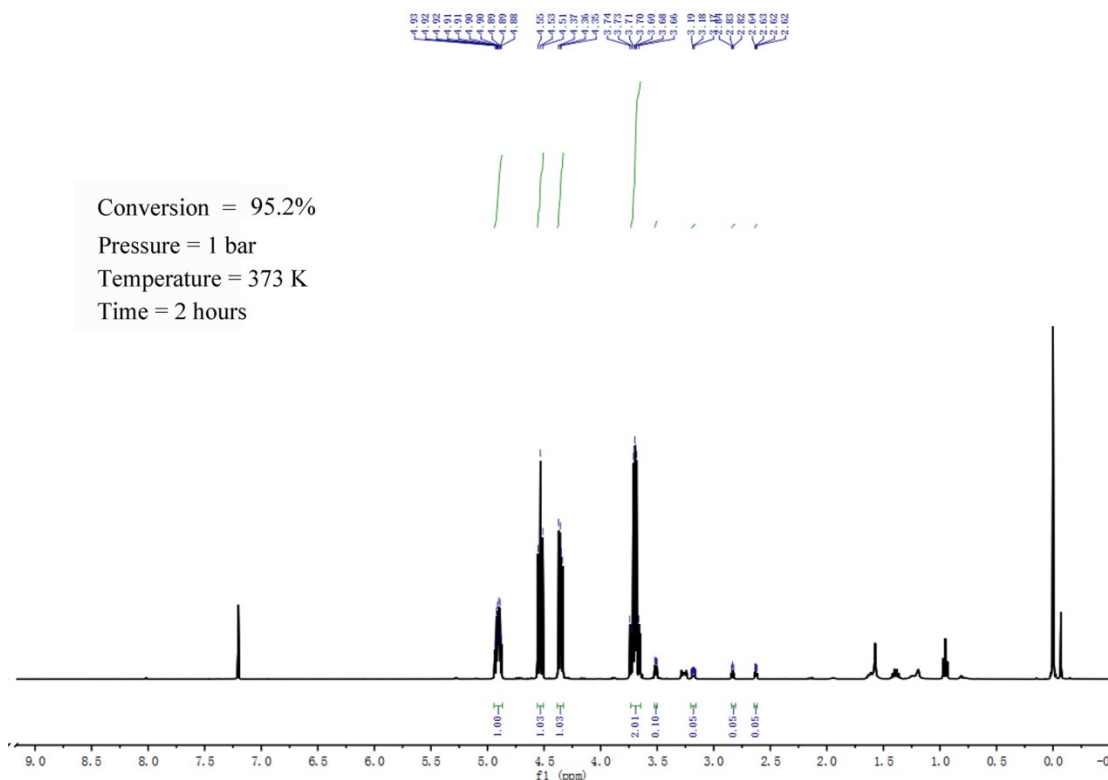
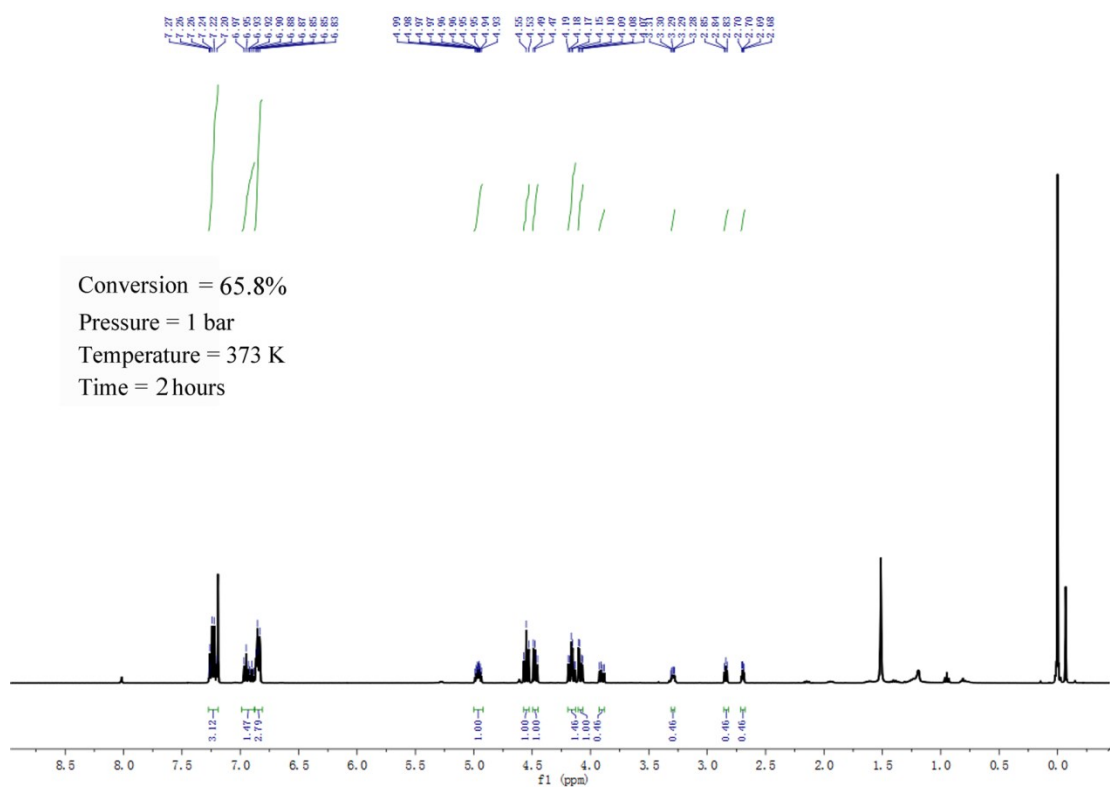
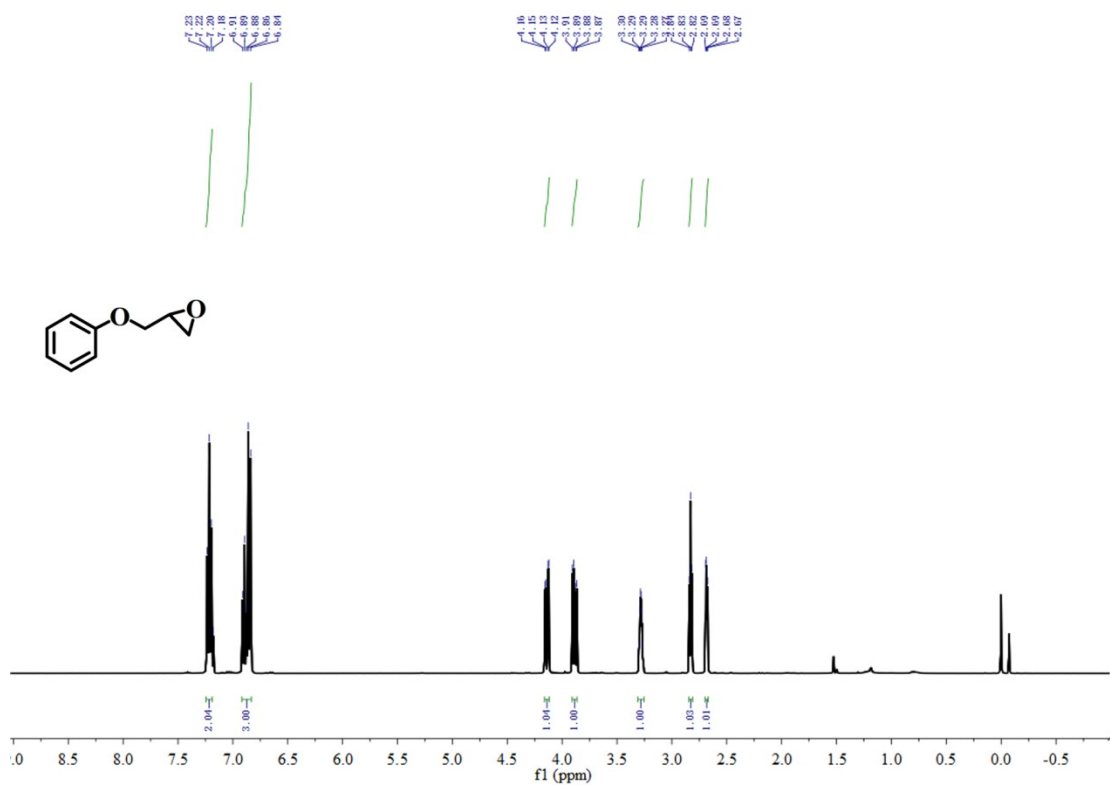


Figure S20 ^1H NMR spectra of the cycloaddition product of chloromethyl-cyclopropane and CO_2 for 2h (400 MHz, CDCl_3): $\delta = 4.88 - 4.93$ (m, 1H, COO-CH), 4.53 (t, $J = 8.0$ Hz, 1H, COO-CH_2), 4.35 (q, $J = 8.0$ Hz, 1H, COO-CH_2), 3.65 – 3.74 (m, 1H, Cl-CH_2 of product), 3.50–3.52 (m, 0.10H, Cl-CH_2 of chloromethyl-cyclopropane), 3.16 – 3.20 (m, 1H, O- CH_2), 2.83 (d, $J = 4.0$ Hz, 1H, O- CH_2), 2.63 (q, $J = 4.0$ Hz, 1H, O- CH_2).



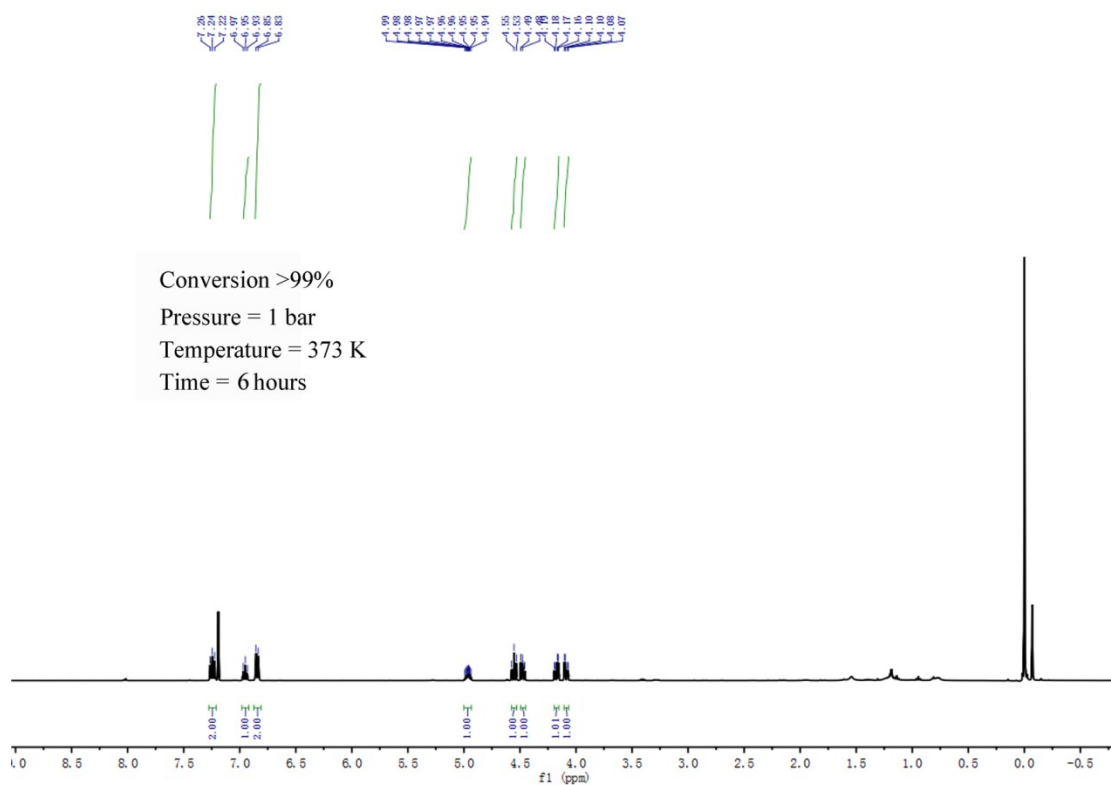


Figure S24 ^1H NMR spectra of the cycloaddition product of 1,2-epoxy-3-phenoxypropane and CO_2 for 6h (400 MHz, CDCl_3): $\delta = 7.24$ (t, $J = 8.0$ Hz, 2H, Ar-H), 6.95 (t, $J = 8.0$ Hz, 1H, Ar-H), 6.84 (d, $J = 8.0$ Hz, 2H, Ar-H), 4.94 – 4.99 (m, 1H, COO-CH), 4.55 (t, $J = 8.0$ Hz, 1H, COO- CH_2), 4.48 (t, $J = 8.0$ Hz, 1H, COO- CH_2), 4.18 (dd, $J = 8.0$ Hz, 4.0 Hz, 1H,ArO- CH_2 of product), 4.08 (dd, $J = 8.0$ Hz, 4.0 Hz, 1H,ArO- CH_2 of product).

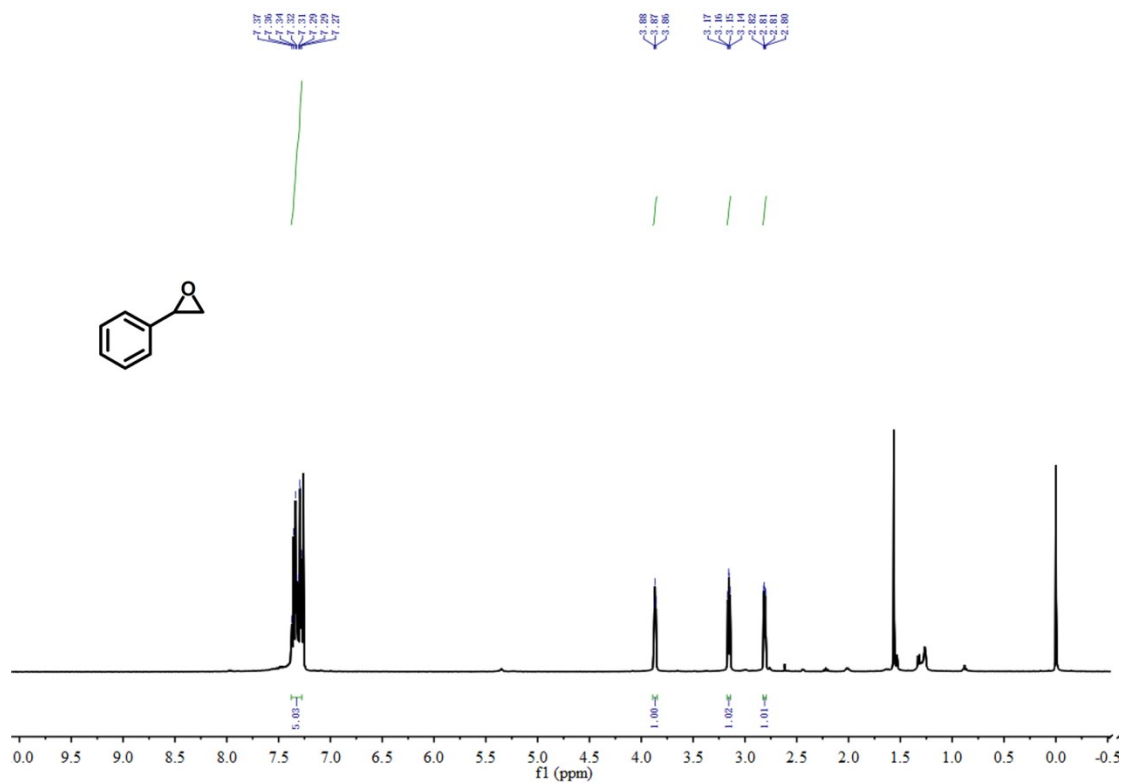


Figure S25 ^1H NMR spectra of styrene oxide (400 MHz, CDCl_3): $\delta = 7.27 - 7.37$ (m, 5H, Ar-H), 3.87 (t, $J=4.0$ Hz, 1H, O-CH), 3.16 (q, $J=4.0$ Hz, 1H, O- CH_2), 2.81 (q, $J = 4.0$ Hz, 1H, O- CH_2).

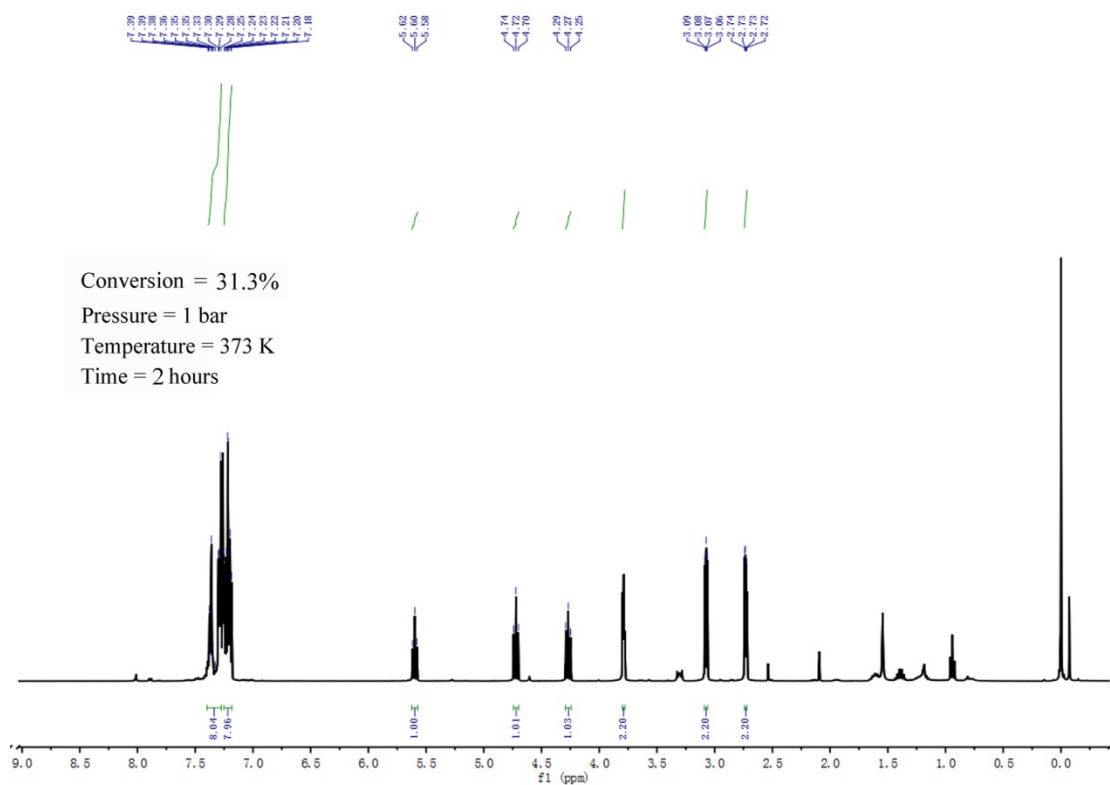


Figure S26 ^1H NMR spectra of the cycloaddition product of styrene oxide and CO_2 for 2h (400 MHz, CDCl_3) : δ = 7.28 – 7.39 (m, 8H, Ar-H), 7.18 – 7.25 (m, 8H, Ar-H), 5.60 (t, J = 8.0 Hz, 1H, COO-CH), 4.72 (t, J = 8.0 Hz, 1H, COO- CH_2), 4.27 (t, J = 8.0 Hz, 1H, COO- CH_2), 3.79 (t, J = 8.0 Hz, 2.20H, O-CH), 3.07 (q, J = 4.0 Hz, 2.20H, O- CH_2), 2.73 (q, J = 4.0 Hz, 2.20H, O- CH_2).

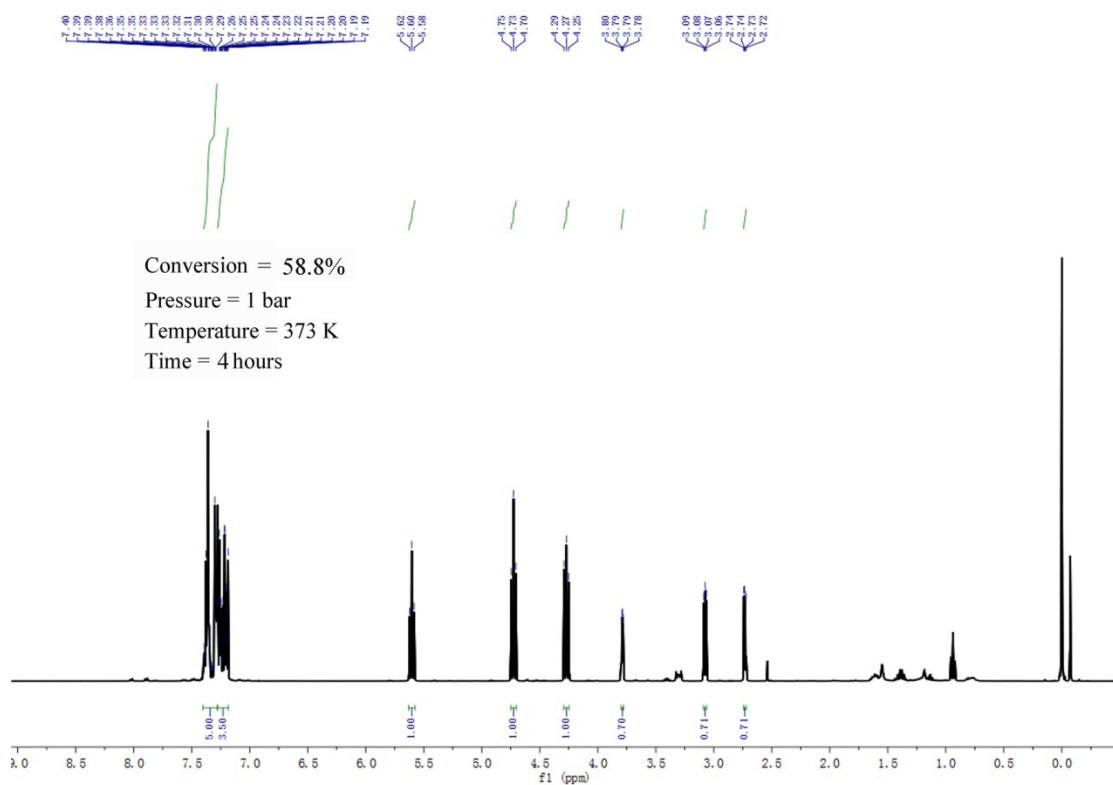


Figure S27 ^1H NMR spectra of the cycloaddition product of styrene oxide and CO_2 for 4h (400 MHz, CDCl_3): δ = 7.29 – 7.38 (m, 5H, Ar-H), 7.19 – 7.26 (m, 2.58H, Ar-H), 5.60 (t, J = 8.0 Hz, 1H, COO-CH), 4.73 (t, J = 8.0 Hz, 1H, COO- CH_2), 4.27 (t, J = 8.0 Hz, 1H, COO- CH_2), 3.79 (q, J = 4.0 Hz, 0.70H, O-CH), 3.08 (q, J = 4.0 Hz, 0.70H, O- CH_2), 2.73 (q, J = 4.0 Hz, 0.70H, O- CH_2).

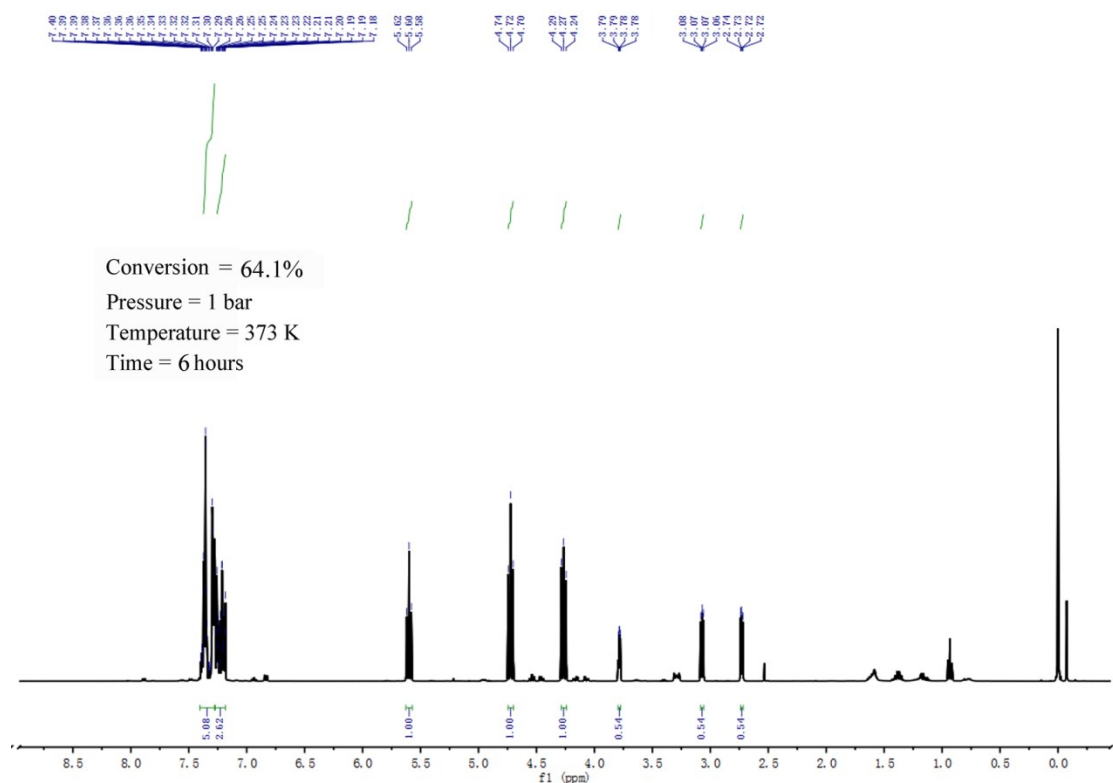


Figure S28 ^1H NMR spectra of the cycloaddition product of styrene oxide and CO_2 for 6h (400 MHz, CDCl_3): δ = 7.29 – 7.40 (m, 5.08H, Ar-H), 7.18 – 7.26 (m, 2.62H, Ar-H), 5.60 (t, J = 8.0 Hz, 1H, COO-CH), 4.72 (t, J = 8.0

Hz, 1H, COO-CH₂), 4.27 (t, J = 8.0 Hz, 1H, COO-CH₂), 3.78 (q, J = 4.0 Hz, 0.54H, O-CH), 3.07 (q, J = 4.0 Hz, 0.54H, O-CH₂), 2.73 (q, J = 4.0 Hz, 0.54H, O-CH₂).

S4. References

References

1. SMART and SAINT software package, Siemens Analytical X-ray Instruments Inc., Madison, WI, 1996.
2. (a) O. V. Dolomanov, L. J. Bourhis, R. J. Gildea, J. A. K. Howard, H. J. Puschmann, *Appl. Cryst.* 2009, **42**, 339–341. (b) G. M. Sheldrick, *Acta Cryst. A*, 2008, **64**, 112–122. (c) G. M. Sheldrick, *Acta Cryst. C*, 2015, **71**, 3–8.
3. V. A. Blatov, *Struct. Chem.* 2012, **23**, 955–963.
4. D. M. Ruthven, *Principles of Adsorption and Adsorption Processes*; Wiley: New York, 1984.
5. A. L. Myers and J. M. Prausnitz, *A.I.Ch.E.J.*, 1965, **11**, 121–127.
6. J.-R. Li, J. Sculley, H.-C. Zhou, *Chem. Rev.* 2012, **112**, 869–932.
7. D. Lässig, J. Lincke, J. Moellmer, C. Reichenbach, A. Moeller, R. Gläser, G. Kalies, K. A. Cychosz, M. Thommes, R. Staudt, H. Krautscheid, *Angew. Chem., Int. Ed.* 2011, **50**, 10344–10348.
8. X.-S. Wang, S.Q. Ma, P. M. Forster, D. Q. Yuan, J. Eckert, J. J. López, B. J. Murphy, J. B. Parise and H.-C. Zhou, *Angew. Chem.* 2008, **38**, 7373–7376 ; *Angew. Chem. Int. Ed.* 2008, **47**, 7263–7266.
9. Z. Guo, H. Wu, G. Srinivas, Y. Zhou, S. Xiang, Z. Chen, Y. Yang, W. Zhou, M. O'Keeffe, B. Chen, *Angew. Chem.* 2011, **123**, 3236–3239; *Angew. Chem. Int. Ed.* 2011, **50**, 3178–3181.
10. X. Lin, J. Jia, X. Zhao, K. M. Thomas, A. J. Blake, G. S. Walker, N. R. Champness, P. Hubberstey, M. Schröder, *Angew. Chem. Int. Ed.* 2006, **45**, 7358–7364.
11. Y. L. Liu, J. F. Eubank, A. J. Cairns, J. Eckert, V. C. Kravtsov, R. Luebcke, M. Eddaoudi, *Angew. Chem. Int. Ed.*, 2007, **46**, 3278–3283.
12. D. De, T. K. Pal, S. Neogi, S. Senthilkumar, D. Das, S. S. Gupta and P. K. Bharadwaj, *Chem. Eur. J.* 2016, **22**, 3387–3396.
13. X. S. Wang, S. Q. Ma, K. Rauch, J. M. Simmons, D. Q. Yuan, X. P. Wang, T. Yildirim, W. C. Cole, J. J. López, A. D. Meijere, and H. C. Zhou, *Chem. Mater.*, 2008, **20**, 3145–3152.
14. X. Lin, I. Telepeni, A. J. Blake, A. Dailly, C. M. Brown, J. M. Simmons, M. Zoppi, G. S. Walker, K. M. Thomas, T. J. Mays, P. Hubberstey, N. R. Champness, M. Schröder, *J. Am. Chem. Soc.* 2009, **131**, 2159–2171.
15. X. Liu, M. Oh, M. S. Lah, *Inorg. Chem.* 2011, **50**, 5044–5053.
16. B. Liu, S. Yao, C. Shi, G. Li, Q. Huo and Y. Liu, *Chem. Commun.*, 2016, **52**, 3223–3226.
17. P. Zhang, B. Li, Y. Zhao, X. Meng, T. Zhang, *Chem. Commun.* 2011, **47**, 7722–7724.
18. Y. Yan, A. J. Blake, W. Lewis, S. A. Barnett, A. Dailly, N. R. Champness, M. Schröder, *Chem. Eur. J.* 2011, **17**, 11162–11170.
19. S. Hong, M. Oh, M. Park, J. W. Yoon, J. S. Chang, M. S. Lah, *Chem. Commun.* 2009, **45**, 5397–5399.
20. M. Dincă, A. Dailly, Y. Liu, C. M. Brown, D. A. Neumann and J. R. Long, *J. Am. Chem. Soc.*, 2006, **128**, 16876–16883.
21. K. Sumida, C. M. Brown, Z. R. Herm, S. Chavan, S. Bordiga, J. R. Long, *Chem. Commun.*

- 2011, **47**, 1157-1159.
22. A. G. W.-Foy, O. Lebel, A. J. Matzger, *J. Am. Chem. Soc.* 2007, **129**, 15740-15741.
 23. X. Zhao, X. Bu, Q.-G. Zhai, H. Tran and P. Feng, *J. Am. Chem. Soc.* 2015, **137**, 1396-1399.
 24. Y.-G. Lee, H. R. Moon, Y. E. Cheon, M. P. Suh, *Angew. Chem. Int. Ed.* 2008, **47**, 7741-7745.
 25. A. O. Yazaydin, R. Q. Snurr, T.-H. Park, K. Koh, J. Liu, M. D. LeVan, A. I. Benin, P. Jakubczak, M. Lanuza, D. B. Galloway, J. L. Low, R. R. Willis, *J. Am. Chem. Soc.* 2009, **131**, 18198-18199.
 26. Z. Bao, L. Yu, Q. Ren, X. Lu, S. Deng, *J. Colloid Interface Sci.* 2011, **353**, 549-556.
 27. X. Guo, G. Zhu, Z. Li, F. Sun, Z. Yang, S. Qiu, *Chem. Commun.* 2006, 3172-3174.
 28. A. O. Yazaydin, A. I. Benin, S. A. Faheem, P. Jakubczak, J. L. Low, R. R. Willis, R. Q. Snurr, *Chem. Mater.* 2009, **21**, 1425-1430.
 29. Y. Hu, S. Xiang, W. Zhang, Z. Zhang, L. Wang, J. Bai, B. Chen, *Chem. Commun.* 2009, 7551-7553.
 30. Z. Zhou, C. He, J. Xiu, L. Yang and C. Duan, *J. Am. Chem. Soc.* 2015, **137**, 15066-15069.
 31. V. Guillerme, Ł. J. Weseliński, Y. Belmabkhout, A. J. Cairns, V. D'Elia, Ł. Wojtas, K. Adil, M. Eddaoudi, *Nature Chem.* 2014, **6**, 673-680.
 32. Y. W. Ren, Y. C. Shi, J. X. Chen, S. R. Yang, C. R. Qi and H. F. Jiang, *RSC Adv.* 2013, **3**, 2167-2170.
 33. H. Y. Cho, D. A. Yang, J. Kim, S. Y. Jeong, W. S. Ahn, *Catal. Today* 2012, **185**, 35-40.
 34. A. C. Kathalikkattil, D. W. Kim, J. Tharun, H. G. Soek, R. Roshan, D. W. Park, *Green Chem.* 2014, **16**, 1607-1616.
 35. J. Song, Z. Zhang, S. Hu, T. Wu, T. Jiang, B. Han, *Green Chem.*, 2009, **11**, 1031-1036.
 36. P.-Z. Li, X.-J. Wang, J. Liu, J.S. Lim, R. Zou, Y. Zhao, *J. Am. Chem. Soc.* 2016, **138**, 2142-2145.